Thin Films of Bismuth Vanadates with Modifiable Conduction Properties

D. Barreca,[†] L. E. Depero,[‡] V. Di Noto,[†] G. A. Rizzi,[†] L. Sangaletti,[‡] and E. Tondello*,[†]

Centro di Studio sulla Stabilità e Reattività dei Composti di Coordinazione del CNR, Dipartimento di Chimica Inorganica, Metallorganica ed Analitica, Università di Padova, Via Marzolo, 1-I-35131 Padova, Italy, and Dipartimento di Chimica e Fisica per i Materiali, Università di Brescia, Via Branze, 38-I-25123 Brescia, Italy

Received June 22, 1998. Revised Manuscript Received October 26, 1998

Thin films of bismuth vanadates are deposited by chemical vapor deposition (CVD) on α-Al_2O_3 substrates using an O_2 atmosphere and vanadyl(IV) acetylacetonate and triphenylbismuth as precursors. The microstructure of the samples is studied by XRD and Raman spectroscopy and their chemical composition is investigated by XPS and SIMS. AFM is used to analyze the surface morphology of the samples. All the samples show a nonohmic behavior beyond a threshold voltage, V_{th}, which is linearly dependent on the V^{4+}/V^{5+} ratio. Impedance spectroscopy measurements indicate that the obtained samples are oxide ion conductors at room temperature and that the mechanism of ion conduction occurs by means of hopping between vacancies. Furthermore, ferroelectric−paraelectric transitions take place in the materials at low temperatures.

Introduction

Great attention has been devoted to the study of the Bi−V−O system in view of its potential applications in many scientific and technological fields. Particularly, bismuth vanadates have been studied as catalysts in oxidation reactions of alkenes and arenes,[1] and their activity has been correlated with the bulk diffusion of lattice oxide ions.[2] In the Bi−V−O system, different crystalline phases exist, depending on the synthesis conditions. The most stable and well-characterized are $BiVO_4$ and $Bi_4V_2O_{11}$.[3]

$BiVO_4$, which is formed by a lattice of corner-sharing BiO_8 dodecahedra and VO_4 tetrahedra,[4] has been reported to be a mixed electronic and ionic conductor with appreciable electronic conductivity at high temperatures.[5] Such mixed conductors are useful in both partial oxidation catalysis and oxygen activation.[6] The $Bi_4V_2O_{11}$ structure is formed by $(Bi_2O_2)^{2+}$ layers interleaved with oxygen deficient perovskite layers $VO_{3.5}^{2-}$.[7] This deficiency in the oxygen sublattice may contribute to the high ionic conductivity measured parallel to the layers.[7] $Bi_4V_2O_{11}$ is also studied for its dielectric, pyroelectric, and ferroelectric properties.[8] The doping of bismuth vanadates with metal ions such as Cu, Mn, V, Mo, and rare earth elements can improve both catalytic and ionic conductor performances of the materials.[9]

Moreover, depending on the composition, glasses of bismuth vanadates have a peculiar nonohmic behavior beyond a threshold voltage and consequently they have been proposed as materials for memory switching devices and electrical rectifiers.[10]

A few examples of mixed Bi−V−O films are reported in the literature.[11] To the best of our knowledge, however, the deposition of thin films of bismuth vanadates has never been carried out by chemical vapor deposition (CVD).

A peculiar advantage of the CVD technique is the possibility to control the composition of the films by varying the partial pressures of the precursors in the vapor phase. In the present study the temperature of the Bi source is changed to prepare by CVD thin films of bismuth vanadates with controlled composition and microstructure. The complexes $VO(acac)_2$ and $BiPh_3$,

* Corresponding author. E-mail: Tondello@Chim02.Chin.Unipd.It. Phone: 0039-49-827-5220. Fax: 0039-49-827-5161.
[†] Università di Padova.
[‡] Università di Brescia.

(1) (a) Ueda, W.; Chen, C.-L.; Asakawa, K.; Moro-Oka, Y.; Ikawa, T. *Chem. Lett*. **1984**, 135. (b) Lee, M.-D.; Chen, W.-S.; Chiang, H.-P. *Appl. Catal. A* **1993**, *101*, 269. (c) Arora, N.; Deo, G.; Wachs, I. E.; Hirt, A. M. *J. Catal*. **1996**, *159*, 1. (d) Bettahar, M. M.; Constentin, G.; Savary, L.; Lavalley, J. C. *Appl. Catal. A: General* **1996**, *145*, 1.
(2) Ueda, W.; Asakawa, K.; Chen, C.-L.; Moro-Oka, Y.; Ikawa, T. *J. Catal*. **1986**, *101*, 360.
(3) Hardcastle, F. D.; Wachs, I. E.; Eckert, H.; Jefferson, D. A. *J. Solid State Chem*. **1991**, *90*, 194.
(4) Granzin, J.; Pohl, D. *Z. Kristallogr*. **1984**, *169*, 289.
(5) Lu, T.; Steele, B. C. H. *Solid State Ionics* **1986**, *21*, 339.
(6) Kendall, K. R.; Navas, C.; Thomas, J. K.; zur Loye, H.-C. *Chem. Mater*. **1996**, *8*, 642.
(7) Touboul, M.; Lokaj, J.; Tessier, L.; Kettman, V.; Vrabel, V. *Acta Crystallogr. B−Struct. Sci*. **1992**, *C48*, 1176.
(8) (a) Prasad, K. V. R.; Varma, K. B. R. *J. Phys. D: Appl. Phys*. **1991**, *24*, 1858. (b) Ramasesha, S. K.; Singh, A. K.; Varma, K. B. R. *Mater. Chem. Phys*. **1997**, *48*, 136. (c) Alga, M.; Wahbi, M.; Ammar, A.; Tanouti, B.; Grenier, J. C.; Reau, J. M. *J. Alloys Compds*. **1997**, *256*, 234.
(9) (a) Abraham, F.; Boivin, J. C.; Mairesse, G.; Nowogrocki, G. *Solid State Ionics* **1990**, *40/41*, 934. (b) Ueda, W.; Chen, C.-L.; Asakawa, K.; Moro-Oka, Y.; Ikawa, T. *J. Catal*. **1986**, *101*, 369. (c) Porta, P.; Lo Jacono, M.; Valigi, M.; Minelli, G.; Anichini, A.; De Rossi, S.; Gazzoli, D. *J. Catal*. **1986**, *100*, 86.
(10) Ghosh, A. *J. Appl. Phys*. **1988**, *64*, 2652 and references therein.
(11) See for instance: (a) Sekiya, T.; Tsuzuki, A.; Torii, Y. *Mater. Res. Bull*. **1985**, *20*, 1383. (b) Pell, J. W.; Ying, J. Y.; zur Loye, H.-C. *Mater. Lett*. **1995**, *25*, 157. (c) Arshak, K.; Perrem, R. *J. Phys. D: Appl. Phys*. **1993**, *26*, 1098.

10.1021/cm980725q CCC: $18.00
Published on Web 01/27/1999

Table 1. Deposition Parameters, Thickness, and Crystal Phases of the Obtained Films[a]

sample	Tp1 (°C)	Tp2 (°C)	thickness (nm)	phases
Bi50	100	50	580	$BiVO_4 + VO_2(B)$
Bi60	100	60	440	$BiVO_4 + VO_2(B)$
Bi65	100	65	370	$BiVO_4 + VO_2(B)$
Bi70	100	70	360	$Bi_4V_2O_{11}$

[a] Substrate temperature = 400 °C; O_2 flow rate = 300 sccm; total pressure = 10 mbar; Tp1 = $VO(acac)_2$ temperature; Tp2 = $BiPh_3$ temperature.

which are commercially available and stable to air and moisture, are used as source compounds. The depositions are carried out in an O_2 atmosphere on polished α-Al_2O_3 at 400 °C. The composition and microstructure of the samples are investigated by X-ray photoelectron spectroscopy (XPS), secondary ion mass spectrometry (SIMS), X-ray diffraction (XRD), and Raman spectroscopy. The surface morphology of the films are analyzed by atomic force microscopy (AFM). A low threshold voltage for nonohmic behavior is evidenced, and correlation among composition, structure, and electrical properties are discussed. A detailed investigation of the electrical properties of these materials as thin films is carried out by impedance spectroscopy (IS).

Results and Discussion

The vapor pressure conditions of the precursors are determined from TGA measurements using the procedure described by Wendlandt.[12] Below 160 °C, the $BiPh_3$ vapor pressure shows a strong dependence on the temperature, while the $VO(acac)_2$ vapor pressure is higher than the $BiPh_3$ vapor pressure and almost constant. Higher temperatures cannot be considered, since the vanadyl complex partly decomposes during volatilization.[13] On the basis of these results, the Bi content of the films is controlled by varying only the temperature of the $BiPh_3$ precursor and fixing the temperature of the $VO(acac)_2$ source at 100 °C.

Deposition parameters, thickness, and phases of the obtained films are reported in Table 1. The temperature of the $BiPh_3$ source during the synthesis is indicated in the label. The color of the films depends on the Bi content, changing from black (low Bi content) to green-yellow (high Bi content).

Morphology. The AFM micrographs (see Figure 1 for sample Bi65) show a rough surface, with a similar texture and an average grain size ranging from 0.30 to 0.50 μm. The average roughness is around 0.06 μm in all samples.

Microstructure and Chemical Composition. In samples Bi50, Bi60, and Bi65 the XRD spectra show the presence of $BiVO_4$ as the main phase with a small amount of $VO_2(B)$ (see Figure 2). This result indicates the presence of an excess of vanadium in the reactive chamber, as expected in view of the relatively high vapor pressure of the vanadyl precursor. The absence of a V_2O_5 phase in the film agrees with our previous study on thin films of vanadium oxides,[14] where only VO_2 phases have been obtained even in oxygen atmosphere. In sample Bi70 only reflections due to $Bi_4V_2O_{11}$ are detected. However, many strong reflections of this phase are absent, as can be observed in Figure 2, where the calculated XRD pattern of the $Bi_4V_2O_{11}$ phase is shown. To clarify this aspect, a simulation of the diffraction pattern was carried out by considering the structure of the Bi_2MoO_6 (i.e., $Bi_4Mo_2O_{12}$) phase with lattice parameters normalized to those of the $Bi_4V_2O_{11}$ cell.[15] In the simulated phase ($Bi_4Mo_2O_{12}$) the Mo ions were substituted by V ions. Moreover, the cation sites were set to be randomly occupied either by V or by Bi. The results are shown in Figure 2. The common feature of the $Bi_4V_2O_{11}$ and $Bi_4Mo_2O_{12}$ phases is the cation sublattice, which was already found to determine the main characteristics of the XRD pattern[16] in mixed Mo−Bi oxides. As can be observed, the simulation resulted in a good agreement with the experimental data.

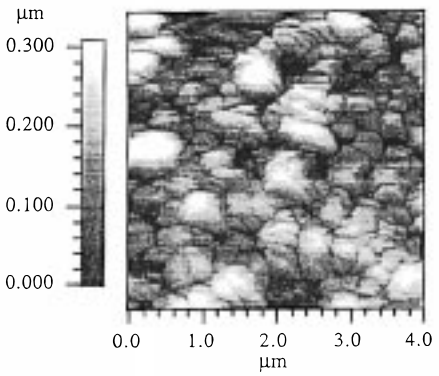

Figure 1. AFM micrograph of sample Bi65 (4 × 4 μm^2).

As a general trend, the structural transformations observed in the present series of samples indicate that the Bi content in the films increases with the temperature of the $BiPh_3$ source (see also XPS data). The Raman spectra, shown in Figure 3, are consistent with the XRD patterns. Indeed, in sample Bi50 the characteristic bands of the $VO_2(B)$ phase[14] can be identified. In the spectra of samples Bi60 and Bi65, the broad band at 830 cm^{-1} is ascribed to V−O stretching in bismuth vanadates,[3] while in sample Bi70 the same band appears at significantly higher wavenumbers (850 cm^{-1}). On the basis of the XRD results, we attribute this change to the presence of the $Bi_4V_2O_{11}$ phase. The broadening of this band may suggest a disorder that, as reported for oxide compounds (see e.g., refs 17 and 18), can be ascribed to different cation−oxygen coordinations or polyhedra distortions in the phase.

Important information about the purity and the surface composition of the samples is obtained by XPS analyses. No surface charging is detected for samples Bi50, Bi60, and Bi65, while in sample Bi70 the electron gun is used to compensate for the charging effect. The conducting behavior of the first three samples may be

(12) Wendlandt, W. WM. *Thermal Analysis*, 3rd ed.; J. Wiley & Sons: Houston, 1985.
(13) Dilli, S.; Patsalides, A. *Aust. J. Chem*. **1976**, *29*, 2369.
(14) Barreca, D.; Depero, L. E.; Franzato, E.; Rizzi, G. A.; Sangaletti, L.; Tondello, E.; Vettori, U. *Electrochem. Soc. Proc.* **1997**, *97−25*, 952.
(15) Lazure, S.; Vannier, R.-N.; Nowogrocki, G.; Mairesse, G.; Muller, C.; Anne, M.; Strobel, P. *J. Mater. Chem*. **1995**, 5, 1395.
(16) Depero, L. E.; Sangaletti, L. *J. Solid State Chem*. **1995**, 119, 428.
(17) Sangaletti, L.; Depero, L. E.; Allieri, B.; Groppelli, S.; Sberveglieri, G. *Mater. Sci. Forum* **1998**, 472, 278.
(18) Sangaletti, L.; Allieri, B.; Depero, L. E.; Bettinelli, M.; Lebbou, K.; Moncorgé, R. paper presented at the 12th International Conference on Crystal growth (ICCG12), Jerusalem, Israel, July 26−31, 1998; to be published in *J. Cryst. Growth*.

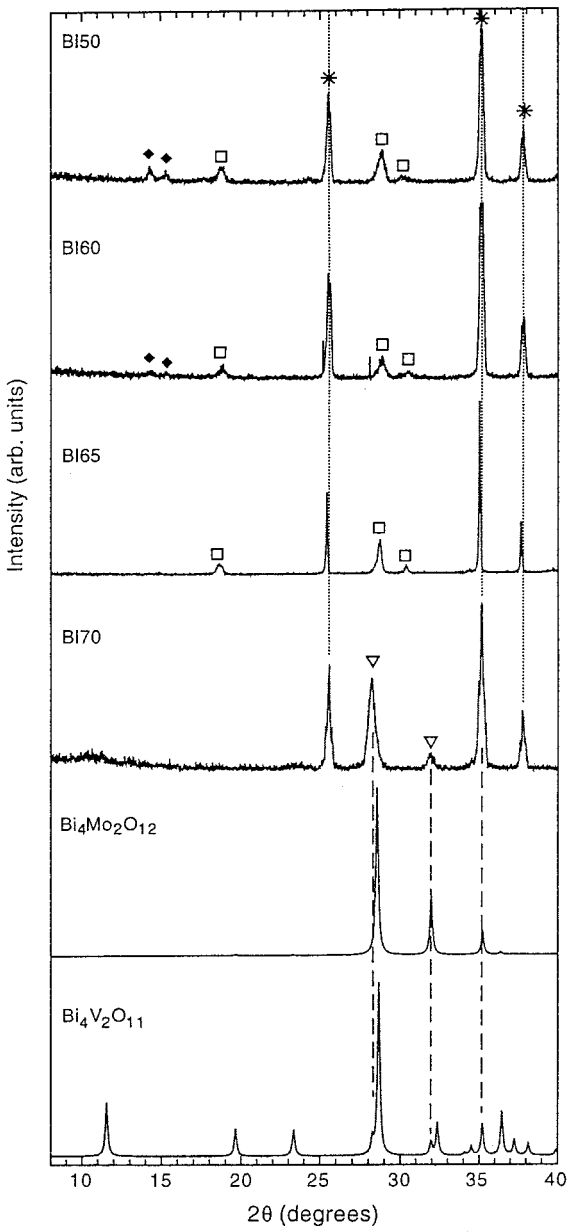

Figure 2. Experimental XRD patterns of the as-grown samples. The symbol * denotes the reflections of the alumina substrate. Reflections belonging to VO_2(B) and $BiVO_4$ are indicated by the symbols ◆ and □, respectively. The calculated XRD patterns of $Bi_4V_2O_{11}$ and $Bi_4Mo_2O_{12}$ are also shown. In the calculation of the XRD pattern of the $Bi_4Mo_2O_{12}$ simulated phase, the Mo ions were subtituted by V ions.

ascribed to the presence of VO_2(B) (n-type semiconductor), detected by XRD and Raman, and to the electrical properties of $BiVO_4$.[19] In Table 2 the V/Bi ratios calculated for all the samples on the basis of the XPS data are reported. A dependence of these values from the temperature of the $BiPh_3$ source is evident, and the high vanadium content in samples Bi50, Bi60, and Bi65 may be related to the ratio of the precursor vapor pressures in the reactor.

The data obtained from XPS surface analysis are summarized in Table 2. The $Bi4f_{7/2}$ peak is found at about 159.4 eV for all samples, a typical value for

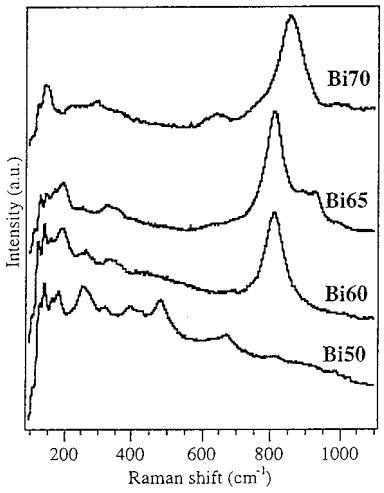

Figure 3. Raman spectra of the as-grown samples.

Table 2. V/Bi Surface Ratio and Binding Energy Data from XPS Analysis

sample	V/Bi	$Bi4f_{7/2}$ (eV)	$V2p_{3/2}(1)$ (eV)	$V2p_{3/2}(2)$ (eV)	V2p fwhm (eV)
Bi50	20.7	159.6	516.1	517.4	2.7
Bi60	9.0	159.6	516.0	517.3	2.3
Bi65	1.2	159.3	516.3	517.1	2.0
Bi70	0.5	159.1	*a*	517.0	1.4

[a] The marked component is not detected.

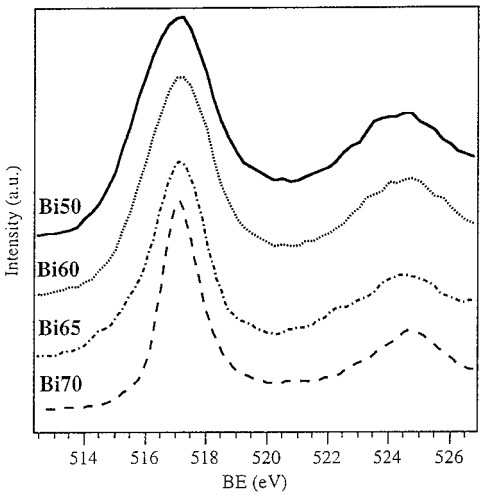

Figure 4. V2p XPS surface peaks for the as-grown samples.

Bi(III) in bismuth vanadates.[20] The V2p XPS peaks are shown in Figure 4. The high fwhm of the $V2p_{3/2}$ peak in sample Bi50 (2.7 eV) may be due to the presence of vanadium in different oxidation states. This peak can be fitted with two components (Table 2): the first, at about 517.2 eV, is ascribed to V(V) in bismuth vanadates;[17] the second, at about 516.0 eV, is assigned to VO_2.[21] Indeed, this second component is not present in Bi70, which is the only sample for which XRD and Raman spectroscopy have not revealed the presence of VO_2(B). Moreover, in this sample the small fwhm of $V2p_{3/2}$ (1.4 eV) and the V/Bi surface ratio confirm the

(19) Hoffart, L.; Heider, U.; Jörissen, L.; Huggins, R. A.; Witschel, W. *Solid State Ionics* **1994**, *72*, 195.

(20) (a) Schuhl, Y.; Baussart, H.; Delobel, R.; Le Bras, M.; Leroy, J. M. *J. Chem. Soc., Faraday Trans. 1* **1983**, *79*, 2055. (b) Le Bras, M.; Agounaou, M.; Gengembre, L.; Baussart, H.; Leroy, J. M. *J. Chim. Phys.* **1996**, *93*, 331.

(21) Mendialdua, J.; Casanova, R.; Barbaux, Y. *J. Electron Spectrosc. Relat. Phenom.* **1995**, *71*, 249.

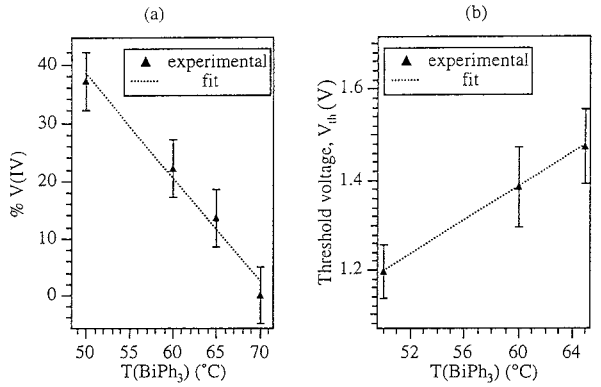

Figure 5. Dependence of vanadium(IV) surface percentage (a) and of threshold voltage (b) on $BiPh_3$ vaporization temperature.

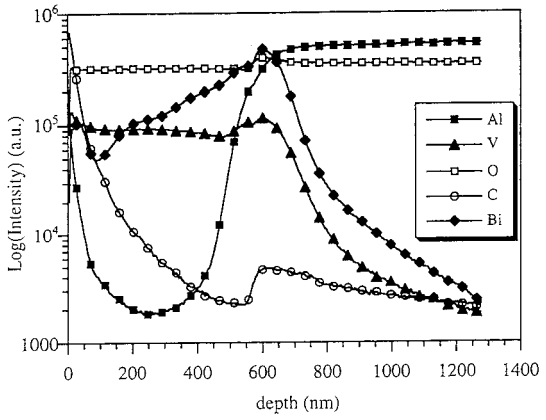

Figure 6. SIMS depth profile of sample Bi50.

presence of only the $Bi_4V_2O_{11}$ phase, as detected by XRD. The relative percentage of V(IV) decreases linearly with the $BiPh_3$ temperature, as shown in Figure 5a.

The SIMS data for samples Bi60, Bi65, and Bi70 (not shown in the figure) indicate that Bi and V profiles have similar shapes, thus confirming the presence of bismuth vanadates as the main phases. The composition of these samples is uniform throughout the entire film depth and a strong diffusion of the film into the substrate is always observed.

In sample Bi50 the species distribution in the matrix is not homogeneous. As shown in Figure 6, the Bi content slowly increases from the surface to the substrate and its profile does not show any correlation with that of vanadium. This indicates that different chemical compounds are present in this film. Indeed, this sample has the greatest VO_2 content, as indicated by XRD and XPS analyses. As shown in Table 1, a greater VO_2 content corresponds to a greater thickness of the obtained films.

Electrical Properties and Impedance Spectroscopy. The $V-I$ curves of the samples Bi50, Bi60, and Bi65 show a linear relationship before a threshold voltage, V_{th}. When $V \geq V_{th}$ the current increases steeply with the potential, indicating a switching to a nonohmic behavior. The values of V_{th} ($\approx$1 V) versus the $BiPh_3$ vaporization temperature can be fitted by a linear function (Figure 5b). A similar I/V behavior has been related, by other authors, to the presence of crystalline VO_2 in the film.[10] This hypothesis is confirmed by the fact that also the V(IV) amount decreases linearly with

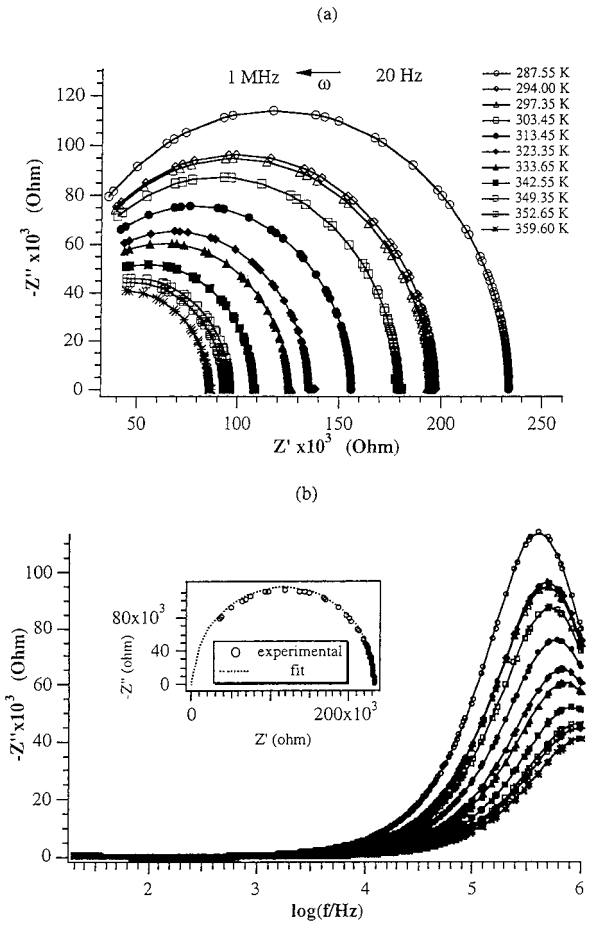

Figure 7. (a) Nyquist plots of sample Bi65 at various temperatures. (b) Imaginary parts of impedance, $-Z''$, versus log[f(Hz)]. The inset shows the experimental Nyquist plot at 287.55 K and the fitted curve obtained by using the EQUIVCRT program written by Boukamp,[24] assuming the model circuit reported in Figure 10b ($\chi^2 = 2 \cdot 10^{-6}$).

the $BiPh_3$ vaporization temperature. The V(IV) centers in a vanadate matrix start the process of dielectric breakdown, which is responsible for the switching to nonohmic behavior.[22] Therefore, an increase of the VO_2 content lowers the threshold voltage. It is clear that sample Bi70, for which no V(IV) can be detected, cannot show such electrical characteristics.

All the samples have been analyzed by IS. However, in the present work we report the results of the analysis performed on sample Bi65, which, from the point of view of the conductivity mechanism, is the most interesting and representative sample. A detailed analysis and discussion of the results obtained by IS will be the subject of a future article.

The dependence of the $-Z''$ vs Z' plot (which is commonly called the Nyquist plot) on temperature, for sample Bi65, is reported in Figure 7a. These profiles are characterized by a single semicircle shape, which is typical for a geometrical capacitance and a bulk resistance in parallel with it.[23] No traces of lower frequency semicircles due to grain boundary impedance are found. A careful analysis of the curves shows that

(22) Rose, R. M.; Shepard, L. A.; Wulff, J. *The Stucture and Properties of Materials*; J. Wiley & Sons: New York, 1966; Vol. 4.
(23) Macdonald, J. R.; Johnson, W. B. *Impedance Spectroscopy*; Mcdonald, J. R., Ed.; J. Wiley & Sons: New York, 1987; p 14.

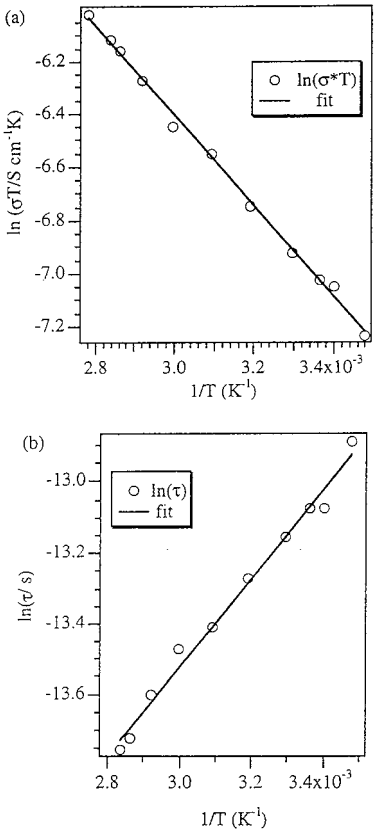

Figure 8. (a) Dependence of $\ln[\sigma T(S\cdot cm^{-1}\cdot K)]$ on temperature for sample Bi65; (b) $\ln[\tau_{peak}(s)]$ versus the inverse temperature for sample Bi65.

two diffusion-limited Warburg impedances are registered in two different temperature ranges. Particularly, in agreement with ref 24, several spikes are observed at low frequency in the ranges 294.0−303.45 and 323.35−342.55 K, suggesting that some structural reorganization, which is source of diffusive processes, could take place in the system, as supported by the analysis of the relative dielectric permittivity reported below. The imaginary component of impendance, Z'', is plotted vs the decimal logarithm of the frequency in Figure 7b, showing a typical Debye peak centered in the $5 \leq \log[f(\text{Hz})] \leq 6$ range.

The complex impedance data, reported in Figure 7a, are fitted satisfactorily by assuming the equivalent circuit shown in Figure 10b. It should be noted that several other equivalent circuits were attempted. For the sake of clarity, we report in the inset of Figure 7b the fitting results carried out on the Nyquist plot at 287.55 K. The dashed line represents the fitted curve, and the value of χ^2 for the final fitting cycle is reported in the figure caption. The fitting was carried out using the EQUIVCRT program written by Boukamp.[24] By assuming the cell constant value reported in the Experimental Section and by using the resistances determined by the fittings, we were able to determine the specific conductivity of sample **Bi65** at various temperatures. As shown in Figure 8a the conductivity of sample Bi65 presents an Arrhenius-type temperature dependence. This behavior is characterized by a preexponential factor $A_\sigma = 0.278 \pm 0.002$ S·cm^{-1} and an activation energy $E_{a,\sigma} = 14.207 \pm 1\cdot10^{-3}$ kJ mol^{-1}. Therefore, the conductivity of sample Bi65 is a thermally activated process and its value at room temperature is ca. $3.3\cdot10^{-6}$ S·cm^{-1}.

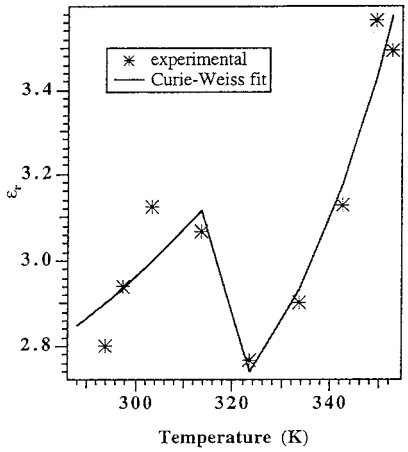

Figure 9. Dependence of the relative dielectric permittivity of sample Bi65 on temperature.

The imaginary part of the impedance exhibits a dielectric relaxation time, $\tau_{peak} = 1/f_{peak}(s)$ (f_{peak} is the frequency at the maximum of the Debye peak), which decreases as the temperature increases (see Figure 7b). An Arrhenius-like behavior is observed plotting $\ln[\tau_{peak}(s)]$ vs $1/T$ (Figure 8b). This phenomenon indicates that a thermally activated relaxation process occurs,[25,26] with an activation energy $E_{a,\tau} = 10.381 \pm 2\cdot10^{-3}$ kJ mol^{-1}. It is interesting to note that $E_{a,\tau}$ is very close to the activation energy $E_{a,\sigma}$ determined by the conductivity Arrhenius plot. This connection suggests that the conductivity in this system is mainly due to a hopping phenomenon.

The relative dielectric permittivity of the system ($\epsilon_r = C/C_o$) is determined as reported in ref 27, where C is the capacity of the sample determined by equivalent circuit fitting on the data of Figure 7a and C_o is the geometrical capacitance of the cell ($C_0 = 2.58\cdot10^{-12}$ F). The dependence of ϵ_r on the temperature (Figure 9) clearly shows the typical pattern exhibited by ferroelectrics[28,29] and is quite well-fitted by the well-known Curie−Weiss equation[30]

$$\epsilon_r = \epsilon_0 + C/(T - T_c)$$

where T_c is the Curie temperature, C is the Curie constant, and ϵ_0 is the high-frequency dielectric constant. The Curie−Weiss fitting parameters in the temperature ranges 287.55 K $\leq T \leq$ 313.45 K and 313.45 K $\leq T \leq$ 347.55 K are reported in Table 3. Now, two facts are to be taken into account: T_c is close to that

(24) Boukamp, B. A. *Equivalent Circuit* (EQUIVCRT. PAS), University of Twente, Department of Chemical Technology, PO Box 217, 7500 AE Enschede, The Netherlands, 1989.

(25) Raistrick, I. D.; Macdonald, J. R.; Franceschetti, D. R. *Impedance Spectroscopy*; Mcdonald, J. R., Ed.; J. Wiley & Sons: New York, 1987; p 48.

(26) Funke, K. *Zeit. Phys. Chem.* **1995**, *188*, 243.

(27) Jonscher, A. K. *Dielectric Relaxation in Solids*; Chelsea Dielectric Press: London, 1983; p 66.

(28) Kittel, C. *Introduction to Solid State Physics*, 5th ed.; Wiley: New York, 1976; Chapter 13, pp 399−431.

(29) Greenwood, N. N.; Earnshaw, A. *Chemistry of the Elements*; Butterworth-Heinemann Ltd: Oxford, 1995; p 60.

(30) Rao, C. N. R.; Gopalakrishnan, J. *New Directions in Solid State Chemistry*, 2nd ed.; Cambridge University Press: 1997; pp 309−310.

Table 3. Curie−Weiss Fitting Parameters[a]

temp range (K)	ϵ_∞	C (K)	T_c (K)
287.55≤ T ≤ 313.45	1.6 ± 0.3	193.3 ± 5.7	437.0 ± 3.3
313.45≤ T ≤ 347.55	1.6 ± 0.2	78.3 ± 1.6	392.4 ± 0.9

[a] The fitting was carried out in the two indicated temperature ranges for sample Bi65.

observed in the ferroelectric compound $BaTiO_3$ (393 K); the ϵ_0 values are similar to those measured in analogues ferroelectric vanadate compounds below the Curie temperature.[31] The main difference between the two temperature ranges is given by the Curie constant values. Since $C \propto J(J + 1)$, where **J** is the total angular momentum of vanadium centers,[30] a variation of C implies a variation of **J**. Hence it is possible that in the system a structural reorganization, with variations of the coordination geometry, takes place in the range 287.55 K ≤ T ≤ 313.45 K, favoring the subsequent ferroelectric−paraelectric transition.

Conclusions

A simple and reproducible procedure for the CVD of bismuth vanadates has been developed. XRD, Raman, and XPS analyses indicate that the composition and microstructure of the samples can be suitably tailored by varying the relative temperatures of the two precursors. An increase in the $BiPh_3$ temperature corresponds to changes from $BiVO_4 + VO_2$ to the $Bi_4V_2O_{11}$ phase. The VO_2 content in the vanadate matrix decreases linearly with the $BiPh_3$ vaporization temperature.

All the samples show a nonohmic behavior beyond a threshold voltage V_{th}, which can be tailored by varying the film composition and is always lower than the values reported in the literature.[10] These properties could be used for the production of electrical rectifiers and memory switching devices with a well-defined threshold voltage.

IS analysis for sample Bi65 shows that at room temperature it exhibits a conductivity of ca. $3.3 \cdot 10^{-6}$ $S \cdot cm^{-1}$. The conductivity is ionic and is due to a hopping mechanism of oxide ions between vacancies, as demonstrated in the dynamic structure model of glasses.[31] Furthermore, a ferroelectric−paraelectric transition is observed for the same sample at low temperatures. A detailed discussion of IS data together with a systematic analysis of the conduction properties of all the samples is in progress and will be published in a future paper.[32]

Experimental Section

Film Deposition. The films were deposited in a two-source cold wall (CW-CVD) reactor using commercially available $BiPh_3$ and $VO(acac)_2$ (Aldrich). Both of these precursors were used as received, since they are stable even in moist air. O_2 was used as carrier and reactive gas. The temperature of the polished α-Al_2O_3 substrate was fixed at 400 °C by a resistively heated susceptor. The precursors were placed in bubblers connected to the reactor tube and heated by two separated oil baths. To avoid condensation of the precursors, gas lines and valves were also heated. The pressure was measured by a capacitance manometer and the gas flow was controlled by a mass flow controller. α-Al_2O_3 substrates (Spec. Tec A493) were ultrasonically degreased in warm trichlorethylene, rinsed in ethanol, and finally dried in oven.

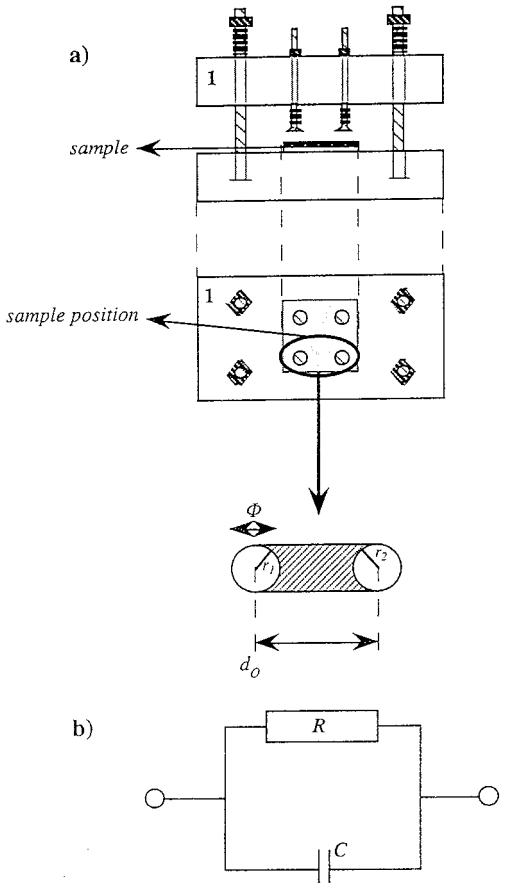

Figure 10. (a) Representation of the cell used for the ac impedance measurements. (b) Equivalent circuit used to model the behavior of impedance spectra of sample Bi65.

TGA. Thermograms of $BiPh_3$ and $VO(acac)_2$ were recorded starting from similar amounts (3−4 mg), using a TGS2 Perkin-Elmer thermobalance at a heating rate of 8 °C/min.

AFM Analysis. Images were collected by using a Park Autoprobe CP instrument in contact mode. The background was subtracted from the images using the ProScan 1.3 software from Park Scientific.

X-ray Diffraction. Diffraction patterns of the thin films were measured by a glancing-incidence diffractometer in an asymmetric Bragg geometry, using Cu Kα radiation and a proportional counter. Structural modeling and simulation of diffraction spectra were performed by the CERIUS program on an IBM RISC 6000 work station.

Micro-Raman Spectroscopy. Micro-Raman spectra were collected with a DILOR Labram spectrometer equipped with a $\lambda = 632.8$ nm He−Ne laser source, a 1800 l/mm grating, and an air-cooled 1024 × 256 pixel CCD detector operating at −70 °C. Rejection of the elastic peak was achieved by a holographic filter, which limited the spectral window at about 150 cm^{-1}. Each spectrum was obtained by averaging 300 scans collected in 1 s each over the 150−1150 cm^{-1} spectral range. After an investigation performed by collecting additional spectra in different areas of the layers, they resulted to be homogeneous on a micron scale.

XPS Analysis. A Perkin-Elmer Φ 5600ci spectrometer with monochromatized Al Kα radiation (1486.6 eV) was used and during the experiments the pressure was less than 1.8×10^{-9} mbar. The spectrometer was calibrated by fixing the binding energy (BE) of the $Au4f_{7/2}$ line at 83.9 eV with respect to the Fermi level. A standard deviation of 0.10 eV in the BE values was evaluated. After a Shirley-type background subtraction, the raw spectra were fitted using a nonlinear least-squares

(31) Lee, C. K.; Sinclair, D. C.; West, A. R. *Solid State Ionics* **1993**, *62*, 193.

(32) Barreca, D.; Di Noto, V.; Rizzi, G. A.; Tondello, E. Work in progress.

fitting program adopting Gaussian−Lorentzian functions for the peak shapes. The atomic compositions were evaluated using sensitivity factors as provided by Φ V5.4A software.

SIMS. Depth profiles were obtained using an ion microscope (CAMECA IMS-4F) equipped with a normal-incidence electron gun used to compensate for the charging effect when profiling insulating samples. The profiles were carried out by 14.5 keV Cs^+ bombardment and by negative ion detection (beam current = 20 nA, raster area = 125 × 125 μm^2). After reaching the substrates, the thickness of the films was measured by an Alpha-Step 200 Tencor profilometer.

Electrical Measurements. *I*−*V* curves were recorded at room temperature by the conventional four point probe method in a Van der Pauw-type arrangement.[33]

IS Measurements. The ac impedance measurements were carried out using a computer-controlled HP4284A Precision LCR meter. The impedance spectra were collected in the frequency region from 20 Hz to 1 MHz and in the temperature range 287.15−363.15 K. A signal voltage of 0.5 V was used. The data were collected using circular gold blocking electrodes laid on the thin films.

The geometry of the cell is shown in Figure 10a. The thin film sample is sandwiched between two Teflon blocks. The upper block is pressed down to the second block by two compression springs. Afterward, the electrodes are gently pressed on the thin film by means of two other weak springs. This arrangement ensures the contact between the electrode interfaces and the thin film at different temperatures and allows us to record impedance spectra avoiding destruction or modification of thin film samples. The cell constant was determined by finite elements method (fem) model and was 1.709 cm. The fem simulations were performed by determining the resistance of an ideal thin sample adopting between electrodes a signal voltage of 0.5 V and a thin film resistivity of $1 \cdot 10^{-6}$ Ω·cm. The distance, d_o, between the centers of the electrodes was 0.610 cm and their radius was $r_1 = r_2 = r =$ 0.167 cm (see Figure 10a). The samples were mounted in the cell in a drybox and kept in a strictly inert argon atmosphere throughout the measuring period.

Acknowledgment. The authors are grateful to Dr. Federico Caccavale of Dipartimento di Fisica-Università di Padova for SIMS measurements and to Mr. G. Greggio for technical assistance.

CM980725Q

(33) Van der Pauw, I. J. *Philips Res. Rep.* **1958**, *13*, 1.